A multi-omic approach reveals iron availability influences cell fate fidelity

Athena Jessica S Ong[1,2], Tara A Tigani[1,2], Jordyn M Reinecke[1], Andrew G Cox[1,2,3*], and Kristin K Brown[1,2,3*]

[1]Peter MacCallum Cancer Centre, Melbourne, Victoria, 3000, Australia
[2]The Sir Peter MacCallum Department of Oncology, The University of Melbourne, Melbourne, Victoria, 3010, Australia
[3]Department of Biochemistry and Pharmacology, The University of Melbourne, Melbourne, Victoria, 3010, Australia

*Equal contribution
Corresponding authors: kristin.brown@petermac.org, andrew.cox@petermac.org

Abstract

Recent evidence has highlighted the importance of employing culture media designed to emulate the metabolic environment Here, we utilize the physiological medium Plasmax to examine the impact of nutrient availability on the human hepatocyte cell line, HepG2. Incubation of HepG2 cells in Plasmax suppressed a transcriptional program driven by Hepatocyte Nuclear Factor 4 (HNF4A), a master regulator of hepatocyte identity. Given that HepG2 cells were originally isolated from a patient with hepatoblastoma, this suggests reversion to the native state in physiological media. Importantly, exclusion of iron from Plasmax reinstated the HNF4A-driven transcriptional program. These studies suggest a relationship between iron availability and the fidelity of hepatocyte cell fate and highlight the importance of more faithfully recapitulating *in vivo* metabolite availability *in vitro*.

Introduction

In vitro cell culture models play a central role in biological and biomedical research. In recent years, efforts to improve the physiological relevance of these models have highlighted the importance of media composition on cellular phenotype and biological responses. For example, the dependence of some cancer cell lines on glutaminolysis is not observed in the *in vivo* context (Davidson *et al*, 2016). This has been attributed to the presence of high cystine concentrations in conventional *in vitro* culture conditions (Muir *et al*, 2017). More generally, conventional media (e.g. Dulbecco's Modified Eagle's Medium, DMEM) poorly recapitulate metabolite levels that cells would be exposed to *in vivo* (Eagle, 1959; Dulbecco & Freeman, 1959). The increasing awareness and recognition that the composition of cell culture media is important in preserving biological processes *in vitro* has led to ongoing efforts to develop cell culture media that better represent physiological metabolite concentrations (Vande Voorde *et al*, 2019; Cantor *et al*, 2017; Tardito *et al*, 2015). Studies employing physiological media have demonstrated that media composition can alter cellular dependencies via metabolic and transcriptional changes (Flickinger *et al*, 2024; Vande Voorde *et al*, 2019; Cantor *et al*, 2017; Apiz Saab *et al*, 2023; Rawat *et al*, 2024; Senkowski *et al*, 2023).

Hepatocytes, the major cell type in the liver, are widely modelled *in vitro* to study drug metabolism, drug-induced liver injury (DILI), and various liver diseases (Kaur *et al*, 2023; Yang *et al*, 2023). The most commonly used cell line in these contexts are HepG2 cells, which were originally derived from a hepatic tumour isolated from a 15-year-old male (Aden *et al*, 1979; Arzumanian *et al*, 2021). Although initially characterised as being derived from a hepatocellular carcinoma (HCC), subsequent histopathologic, genetic and molecular analysis revealed that the origin of HepG2 cells was instead from a hepatoblastoma (HB) (López-Terrada *et al*, 2009). Despite this, HepG2 cells are still widely utilized as a hepatocyte cell line as they exhibit the hallmarks of hepatocyte fate and function *in vitro* (Liu *et al*, 2022, 2021; Lin *et al*, 2016; Park *et al*, 2018; Zhang *et al*, 2018).

In this study, we examined the impact of nutrient availability on HepG2 cells by comparing culture in conventional media with culture in a media previously developed to more faithfully reflect metabolite abundance in human plasma (Plasmax) (Vande Voorde *et al*, 2019). We demonstrate that culturing HepG2 cells in Plasmax alters cell fate in a manner associated with loss of HNF4A. Moreover, we demonstrate that iron availability contributes to the regulation of hepatic cell fate. This research suggests an important role for physiological media in maintaining cell fate *in vitro*.

Results

HepG2 cells adopt a native hepatoblast-like state in physiological media

Typically, HepG2 cells are maintained in one of three conventional cell culture media: EMEM, high glucose DMEM (HG-DMEM) or low glucose DMEM (LG-DMEM) (Sanghvi *et al*, 2019; Chen *et al*, 2024; Jiang *et al*, 2023; Ong *et al*, 2023). To examine the impact of culture media on the transcriptional landscape, HepG2 cells were cultured in each of the three conventional media types or in the physiological medium Plasmax (Vande Voorde *et al*, 2019). Plasmax mimics metabolite concentrations found in human plasma and has a dramatically different composition than conventional cell culture media (Fig. S1A). While minimal transcriptional changes were observed in response to culture in any of the three conventional media, culture in Plasmax induced widespread transcriptional changes (Fig. S1B,C). Amongst the most significant changes observed in Plasmax, relative to EMEM, was upregulation of the pioneer transcription factor SRY-Box Transcription Factor 4 (*SOX4*), a regulator of hepatocyte dedifferentiation, and concomitant downregulation of genes (Apolipoprotein H, *APOH*; Albumin, *ALB*; Transferrin, *TF*) controlled by Hepatocyte Nuclear Factor 4 Alpha (HNF4A), a transcription factor that regulates hepatocyte identity (Fig. 1A) (Parviz *et al*, 2003; Sekiya & Suzuki, 2011; Katsuda *et al*, 2024). Downregulation of HNF4A in Plasmax was confirmed at the level of protein expression (Fig. 1B). Consistent with these observations, Gene Set Enrichment Analysis (GSEA) revealed downregulation of signatures associated with hepatocyte cell state and hepatocyte function in the context of culture in Plasmax (Fig. 1C). In the developmental context, hepatoblasts are bipotential progenitor cells that differentiate to give rise to both hepatocytes and cholangiocytes (Fig. S1D) (Gordillo *et al*, 2015). Culture in Plasmax induced an increase in the expression of genes associated with a hepatoblast-like state (e.g. Epithelial Cell Adhesion Molecule, *EPCAM* and SRY-Box Transcription Factor 9, *SOX9*) and, as previously mentioned, loss of genes associated with differentiated hepatocytes (e.g. *ALB*, *APOH*, and *TF*) suggesting that culture in physiological media drives dedifferentiation (Fig. 1D). In contrast, culture of the HCC-derived hepatocyte cell line Hep3B in Plasmax did not impact HNF4A protein expression (Fig, S1E). This was expected as Hep3B cells are not derived from HB and represent an intrinsically differentiated hepatocyte cell line. Finally, analysis of a publicly available dataset examining the impact of culture conditions on the basal-like breast cancer cell line MDA-MB-468 revealed a shift to a progenitor-like state when cells were cultured in Plasmax (Fig. S1F) (Vande Voorde *et al*, 2019; Charafe-Jauffret *et al*, 2006; Neve *et al*, 2006). Overall, these data suggest that culture in physiologic media maintains cell fate fidelity *in vitro*.

102 **Trace element availability regulates hepatocyte differentiation**

103 To examine the components of Plasmax contributing to dedifferentiation of HepG2
104 cells, variants of Plasmax lacking either trace elements, which are severely underrepresented
105 in EMEM/DMEM, or lacking metabolites absent from EMEM/DMEM (termed "supplemental
106 metabolites") were prepared (Fig. S1A) (Vande Voorde *et al*, 2019). Withdrawal of trace
107 elements, but not supplemental metabolites, restored HNF4A protein expression to levels
108 observed in EMEM (Fig. 2A). Moreover, transcriptomics revealed that trace element
109 withdrawal restored hepatocyte gene expression and expression of signatures associated with
110 hepatocyte cell state and hepatocyte function (Fig. 2B,C). Notably, *SOX4* expression was
111 suppressed and returned to levels observed in EMEM when cells were cultured in Plasmax
112 devoid of trace elements (Fig. 2C,D).

113

114 **Multi-omics analysis reveals a relationship between trace element availability and**
115 **metalloprotein expression**

116 To gain insights regarding which trace element(s) was contributing to dedifferentiation
117 in Plasmax, intracellular trace element abundance was quantified using inductively-coupled
118 plasma mass spectrometry (ICP-MS). Given that serum can be a source of trace elements,
119 trace elements were also quantified in fresh culture media. As expected, trace elements were
120 elevated in Plasmax compared to EMEM (Fig. S2A). Interestingly, despite iron levels being
121 increased by only four-fold in Plasmax relative to EMEM, HepG2 cells cultured in Plasmax
122 exhibited more than a twenty-fold increase in intracellular iron (Fig. 3A). A three-fold increase
123 in intracellular copper was also observed (Fig. 3A). To explore the role of iron in hepatocyte
124 differentiation, iron salts were added back to Plasmax devoid of trace elements. A
125 multidimensional scaling (MDS) plot of the transcriptome revealed that while withdrawal of
126 trace elements from Plasmax resulted in a transcriptome more similar to EMEM, reintroduction
127 of iron resulted in a transcriptome that was more similar to Plasmax (Fig. 3B). This trend was
128 recapitulated at the proteome level where reintroduction of iron restored a proteomic profile
129 similar to HepG2 cells incubated in complete Plasmax (Fig. 3C). Interestingly, a correlation
130 plot of the transcriptome and proteome of cells cultured in Plasmax lacking trace elements
131 compared to complete Plasmax revealed proteins that were significantly downregulated at the
132 protein, but not the transcript, level in response to removal of trace elements. Notably, among
133 these proteins were selenoproteins (e.g. Selenoprotein P, *SELENOP* and Glutathione
134 Peroxidase 1, *GPX1*) and iron-regulated proteins (e.g. Ferritin Heavy Chain 1, *FTH1*) (Fig.
135 3D). These proteins belong to the metalloprotein superfamily and their translation is dependent
136 on trace element availability (Copeland, 2003; Addess *et al*, 1997). Consistent with this,
137 addition of iron salts to Plasmax devoid of trace elements was able to rescue the expression
138 of iron-regulated proteins but not selenoproteins, demonstrating the importance of trace

139 elements in the post-transcriptional regulation of protein abundance (Fig. 3E). Taken together,
140 these results highlight a role for trace elements in the regulation of cellular phenotype and
141 demonstrate the importance of utilizing a multi-omic approach to interrogate the impact of
142 altered nutrient availability.
143
144 **Iron availability contributes to the regulation of hepatocyte cell fate**
145 Given that the intracellular levels of iron and copper were significantly increased in
146 HepG2 cells cultured in Plasmax (Fig. 3A), these trace elements were further examined for
147 their role in modulating hepatocyte cell fate. Interestingly, reintroduction of iron salts, but not
148 copper salts, to Plasmax devoid of trace elements suppressed HNF4A expression (Fig. 4A).
149 Moreover, re-introduction of iron salts suppressed signatures associated with the differentiated
150 hepatocyte cell state (Fig. 4B,C). The majority of labile iron is incorporated in the cofactor
151 heme(Ajioka *et al*, 2006). The transcriptional repressor BTB and CNC Homolog 1 (BACH1)
152 plays a central role in regulating intracellular heme homeostasis and is itself regulated by
153 heme availability (Oyake *et al*, 1996; Ogawa *et al*, 2001; Sun *et al*, 2002). Interestingly, BACH1
154 has also been shown to contribute to the regulation of cell fate (Wei *et al*, 2019; Oyake *et al*,
155 1996). Notably, proteomics analysis revealed that BACH1 target genes were upregulated after
156 reintroduction of iron salts to Plasmax devoid of trace elements (Fig. 4D). Finally, BACH1
157 protein expression was dramatically lower in HepG2 cells cultured in Plasmax versus EMEM
158 (Fig. 4E). Taken together, these data suggest that the iron-dependent dedifferentiation of
159 hepatocytes in Plasmax is mediated by the trace element iron through regulation of the
160 transcription factor BACH1 (Fig. S3A).
161
162 **Discussion**
163 The liver biopsy from which HepG2 cells were isolated in 1979 was described as a well
164 differentiated HCC (Aden *et al*, 1979). It was not until 2009 when the histopathology and
165 genetics of the original biopsy was revisited that it was reclassified as a HB (López-Terrada *et*
166 *al*, 2009). Despite this correction, HepG2 cells are still widely used to model hepatocytes/HCC
167 rather than hepatoblasts/HB (Liu *et al*, 2022, 2021; Lin *et al*, 2016; Park *et al*, 2018; Zhang *et*
168 *al*, 2018). This is reasonable as HepG2 cells cultured in conventional media exhibit
169 characteristics consistent with differentiated hepatocytes (Fig. 1C). In this study, we have
170 demonstrated that incubation in a physiological medium, Plasmax, causes HepG2 cells to
171 revert to their native hepatoblast state.
172 A previous study investigating the impact of cell culture conditions on HepG2 cells
173 demonstrated that increased amino acid availability promoted the acquisition of a
174 transcriptome similar to primary human hepatocytes (Boon *et al*, 12/2020). In other cell lines,
175 physiologically relevant metabolites that are underrepresented or absent in conventional

176 media, such as urea and the trace element selenium, have been shown to drive significant
177 changes in cell metabolism (Cantor *et al*, 2017; Vande Voorde *et al*, 2019). Here, we have
178 shown that underrepresentation of the trace element iron in conventional media drives
179 differentiation of HepG2 cells to a hepatocyte state. Maintenance of intracellular iron
180 homeostasis has been shown to play a role in determining fate in other cell types including
181 breast cancer cells, hematopoietic stem cells and alveolar cells (Kao *et al*, 2024; Zhuang *et*
182 *al*, 2025; Müller *et al*, 2020). Although trace elements exist in minute quantities in the plasma,
183 these studies highlight the importance of considering trace element availability when
184 employing cell culture models.

185 We demonstrate that removal of trace elements from Plasmax triggers the
186 downregulation of proteins harbouring iron response elements in the 5'-UTR of the associated
187 transcripts (IRE; e.g. ACO2, FTL, FTH1) (Aziz & Munro, 1987; Hentze *et al*, 1987; Shen *et al*,
188 2023). IREs are recognized by IRE binding proteins, which in the absence of iron, repress
189 protein expression by hindering the binding of translation initiation factors (Gray & Hentze,
190 1994). In addition to iron, the availability of other trace elements can dramatically impact the
191 proteome. For example, the translation of selenoproteins, which contain the cysteine analogue
192 selenocysteine (Sec), is dependent on selenium availability (Zinoni *et al*, 1986; Chambers *et*
193 *al*, 1986; Copeland, 2003; Kryukov *et al*, 2003). Since the protein expression of IRE-containing
194 proteins and selenoproteins are regulated at the translational level, changes in their
195 expression resulting from altered trace element availability would not be detected at the
196 transcriptional level. This underscores the importance of employing multi-omic approaches to
197 investigate the consequences of altering metabolite availability.

198 BACH1 is a transcription factor that regulates iron homeostasis and is highly
199 responsive to changes in iron availability (Kitamuro *et al*, 2003; Chen *et al*, 2023). Interestingly,
200 in lung cancer, BACH1 has been shown to drive changes in cell plasticity via epithelial-to-
201 mesenchymal transition (Wiel *et al*, 2019; Lignitto *et al*, 2019). Moreover, BACH1 has been
202 shown to interact with transcription factors that regulate self-renewal (e.g. NANOG, SOX2,
203 and OCT4) to repress transcription of mesodermal genes and promote pluripotency in human
204 embryonic stem cells (Wei *et al*, 2019). Our findings demonstrate that BACH1 is
205 downregulated in HepG2 cells cultured in Plasmax (Fig. 4E). Future studies investigating the
206 interplay between iron availability, BACH1 and cell fate are warranted.

207 In conclusion, our study adds to a growing body of literature highlighting the importance
208 of more faithfully recapitulating the *in vivo* metabolic microenvironment when employing *in*
209 *vitro* cell culture models. Considering these findings, we suggest that, in addition to providing
210 an opportunity to identify novel modulators of cell fate, physiological media will improve the *in*
211 *vivo* relevance of *in vitro* cell culture models by maintaining cell fate fidelity *in vitro*.
212

213 **Materials and Methods**

214 **Cell culture**

215 HepG2 cells were purchased from the European Collection of Authenticated Cell Cultures
216 (ECACC) via CellBank Australia and Hep3B cells were purchased from American Type Culture
217 Collection (ATCC). Both cell lines were routinely assayed for mycoplasma contamination.
218 Cells were cultured in high glucose DMEM (DMEM-HG; Thermo Fisher Scientific, 11965118),
219 low glucose DMEM (DMEM-LG; Thermo Fisher Scientific, 11885084), Plasmax (prepared in-
220 house as previously described (Vande Voorde *et al*, 2019)) or EMEM, which was prepared by
221 supplementing MEM, NEAA, no glutamine (Thermo Fisher Scientific, 10370) with 1 mM
222 sodium pyruvate, 2 mM glutamine. Cells were maintained in a humidified incubator at 37°C
223 with 5% CO_2. For all experiments, $2x10^5$ HepG2 cells and $8x10^4$ Hep3B cells were seeded in
224 6-well plates in EMEM containing 10% heat-inactivated FBS (HyClone™, SH30084). 24 hours
225 after seeding, wells were washed with PBS and the appropriate media (DMEM-HG, DMEM-
226 LG, Plasmax or EMEM) containing 10% heat-inactivated FBS was added. Media was
227 refreshed after 48 hours and cells were harvested 96 hours after transition to the different
228 media types.

229

230 **RNA-Seq analysis**

231 For RNA-Seq analysis, total RNA was extracted using the NucleoSpin RNA kit (Macherey-
232 Nagel, 740955) as per manufacturer's instructions. RNA quality was confirmed using an
233 Agilent 4200 TapeStation System. Libraries were prepared using the QuantSeq 3' mRNA-Seq
234 kit (Lexogen, 015) and sequenced with an Illumina NextSeq 500, with single-end 75 bp reads
235 to a depth of 5 M reads per sample. FASTQ files were uploaded to the Galaxy web platform
236 for quality control (FastQC), trimming (Cutadapt), alignment (RNA STAR), and counting
237 (featureCounts) (Afgan *et al*, 2016). Reads were aligned to the human genome assembly
238 (Ensembl hg19, GRCh37). Analysis of differentially expressed genes was performed with
239 Limma-Voom (v3.40.6) (Smyth, 2005; Law *et al*, 2014). Gene set enrichment analysis (GSEA)
240 was performed and plotted in R using the 'clusterProfiler' package (Yu *et al*, 2012). Heatmaps
241 and volcano plots were generated in R using the 'pheatmap' and 'ggplot' packages
242 respectively(Kolde, 2012; Wickham, 2016).

243

244 **Quantitative polymerase chain reaction (qPCR)**

245 Total RNA was isolated using the NucleoSpin RNA Kit (Macherey-Nagel, 740955) following
246 manufacturer's instructions. Complementary DNA (cDNA) was synthesized using the High-
247 Capacity cDNA Reverse Transcription Kit (Thermo Fisher Scientific, 4368813) according to
248 the manufacturer's guidelines. cDNA was diluted 5-fold in nuclease-free H_2O (Thermo Fisher
249 Scientific, 10977015). qPCR was performed using Applied Bioystems Fast SYBR™ Green

250 Master Mix (Thermo Fisher Scientific, 4385616) and the Applied StepOnePlus Real-Time PCR
251 System (Thermo Fisher Scientific). Primers for *RPLP0* (5'-CAGATTGGCTACCCAACTGTT-3'
252 and 5'-GGGAAGGTGTAATCCGTCTCC-3'), *ALB* (5'-CTTGAATGTGCTGATGACAGG-3' and
253 5'-GCAAGTCAGCAGGCATCTCAT-3'), and *ACAT2* (5'-GCGGACCATCATAGGTTCCTT-3'
254 and 5'- CTGCAAGGCACACAGCTTTT-3') were used for qPCR. Relative gene expression was
255 determined using the ΔΔCt method(Rao *et al*, 2013) normalised to *RPLP0*.
256
257 **Immunoblotting**
258 Cells were washed with PBS and lysed in SDS lysis buffer (1% SDS, 50 mM Tris-HCl, 10 mM
259 EDTA) containing a protease inhibitor cocktail (Sigma-Aldrich, P8340) and Pierce™ Universal
260 Nuclease for Cell Lysis (Thermo Fisher Scientific, 88072). Lysates were resolved by SDS-
261 PAGE and transferred to nitrocellulose membrane. Membranes were probed with primary
262 antibodies recognising HNF4A (Cell Signaling Technology, 3113, 1:1000 dilution), BACH1
263 (Proteintech, 14018-1-AP, 1:500 dilution), and β-Actin (Cell Signalling Technology, 3700,
264 1:5000 dilution). Membranes were incubated with IRDye secondary antibodies (LI-COR, 926-
265 68070 and 926-32211) and imaged using the Odyssey DLx imaging system (LI-COR).
266
267 **Inductively-coupled plasma mass spectrometry (ICP-MS)**
268 ICP-MS was performed as previously described(Pyun *et al*, 2022). Cells were washed with
269 PBS and whole cell lysates were collected in SDS lysis buffer. Media with 10% FBS (500 μL)
270 was used to determine trace element abundance in EMEM and Plasmax. Lysates or media
271 were lyophilized prior to digestion in 65% nitric acid (Merck, 100441). Samples were heated
272 at 90˚C for 20 minutes to complete the digestion and subsequently diluted with 1% (v/v) nitric
273 acid. Samples were run on the Agilent 8800 (ICPMS-QQQ-8800) system using a Helium
274 reaction gas cell. Raw parts per billion (ppb) data of the elements were converted to μmol/L
275 with dilution factors applied. The final concentrations of the metals were corrected with the
276 treatment blanks and normalized to the total protein to obtain a final unit expressed as
277 metal/mg protein. Fold changes were normalized to the average of controls.
278
279 **Proteomic Analysis**
280 Cells were washed with PBS and lysed in 200 μL of ice-cold RIPA buffer (1% NP-40, 0.5%
281 sodium deoxycholate, 0.1% SDS, 150 mM NaCl, 50 mM Tris-HCl, pH 7.5) containing a
282 protease-inhibitor cocktail (Sigma-Aldrich, P8340) and phosphatase inhibitors (Roche,
283 4906845001). Protein (50 μg per sample) was reduced by adding a final concentration of 10
284 mM TCEP (Sigma-Aldrich, 646547) and incubated at 37˚C for 45 min. Samples were then
285 alkylated with 50 mM iodoacetamide (Sigma-Aldrich, I1149) and incubated in the dark for 45
286 min. After acidification with 2.5% phosphoric acid (Sigma-Aldrich, 79617), samples were

287 passed through S-Trap micro columns (Protifi, C02-micro). Proteins were digested overnight
288 at 37˚C with a 1:20 dilution of Pierce™ Trypsin Protease (Thermo Fisher Scientific, 90057).
289 Peptides were eluted sequentially with 50 mM triethylammonium bicarbonate buffer (TEAB),
290 0.2% formic acid, and 50% acetonitrile/0.2% formic acid. Finally, the eluent was lyophilized
291 and reconstituted in 2% acetonitrile/0.05% trifluoroacetic acid to make up the peptide solution
292 for LC-MS/MS analysis by data-independent acquisition using a Thermo OrbiTrap Ascend
293 mass spectrometer. Data analysis was performed using the software suite, DIA-NN (Demichev
294 *et al*, 2020). Heatmaps and volcano plots were generated in R using the 'pheatmap' and
295 'ggplot' packages respectively (Kolde, 2012; Wickham, 2016).
296
297 **Quantification and Statistical Analysis**
298 Statistical analyses were performed with Prism 9 software (GraphPad Software). All statistical
299 analyses for data comparing two groups were performed with an unpaired Student's t-test.
300 One-way ANOVA with the Holm–Sidak method for multiple comparisons was used for
301 comparison of more than two groups. All immunoblots are representative of results from at
302 least three independent experiments. All other statistical details of experiments can be found
303 in the figure legends.
304
305 **Acknowledgements**
306 A.J.S.O. is supported by a Peter MacCallum Cancer Centre Foundation Grant. T.A.T. is
307 supported by an Australian Government Research Training Program Scholarship. K.K.B. is
308 supported by NHMRC Ideas Grants (GNT2004212 and GNT2012313) and a Victorian Cancer
309 Agency Mid-Career Research Fellowship (MCRF17020). A.G.C. is supported by a National
310 Health and Medical Research Council (NHMRC) Investigator Grant (GNT1176650), and an
311 Australian Research Council Discovery Project Grant (DP200102693). K.K.B and A.G.C. are
312 also jointly supported by the Peter MacCallum Cancer Foundation (Ted and Lila Seehusen
313 Foundation). We acknowledge support from the Peter MacCallum Cancer Centre Foundation
314 and the Australian Cancer Research Foundation. We acknowledge the Bio21 Melbourne Mass
315 Spectrometry and Proteomics Facility (MMSPF) at the University of Melbourne and the
316 Biometals Facility at the Florey Institute of Neuroscience and Mental Health (University of
317 Melbourne) for their training, support, and technical assistance. We extend our thanks to the
318 Peter MacCallum Cancer Centre Core Facilities and their staff who provided support for this
319 work; namely the Molecular Genomics Core, the Flow Cytometry Core and the Bioinformatics
320 Core Facilities. Finally, we thank members of the Cox Laboratory and Brown Laboratory (Peter
321 MacCallum Cancer Centre) for helpful discussions.
322
323 **Author contributions**

A.J.S.O., A.G.C., and K.K.B. designed research; A.J.S.O., T.A.T., and J.M.R. performed research; A.J.S.O. analyzed data; A.G.C. and K.K.B. supervision; and A.J.S.O., A.G.C., and K.K.B. wrote the paper.

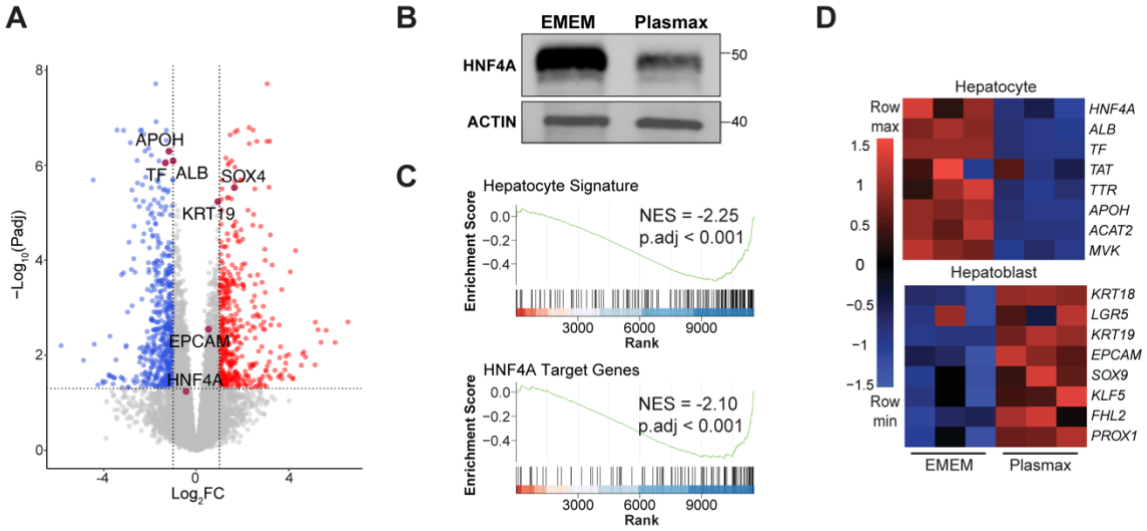

Figure 1. HepG2 cells adopt a native hepatoblast-like state in physiological media. (A) Volcano plot of differentially expressed genes (DEGs) identified from RNA-Seq analysis comparing HepG2 cells cultured in Plasmax with HepG2 cells cultured in EMEM, n=3. Hepatocyte differentiation markers are highlighted in maroon. Significantly upregulated genes are highlighted in red. Significantly downregulated genes are highlighted in blue. (B) Representative immunoblot analysis of HepG2 cells cultured in EMEM or Plasmax. (C) Gene set enrichment analysis (GSEA) plots derived from RNA-Seq analysis comparing HepG2 cells cultured in Plasmax with HepG2 cells cultured in EMEM demonstrating signatures associated with hepatocyte cell state and function. (D) Heatmap of hepatocyte and hepatoblast gene expression in HepG2 cells culture in EMEM or Plasmax as determined by RNA-Seq analysis, n=3.

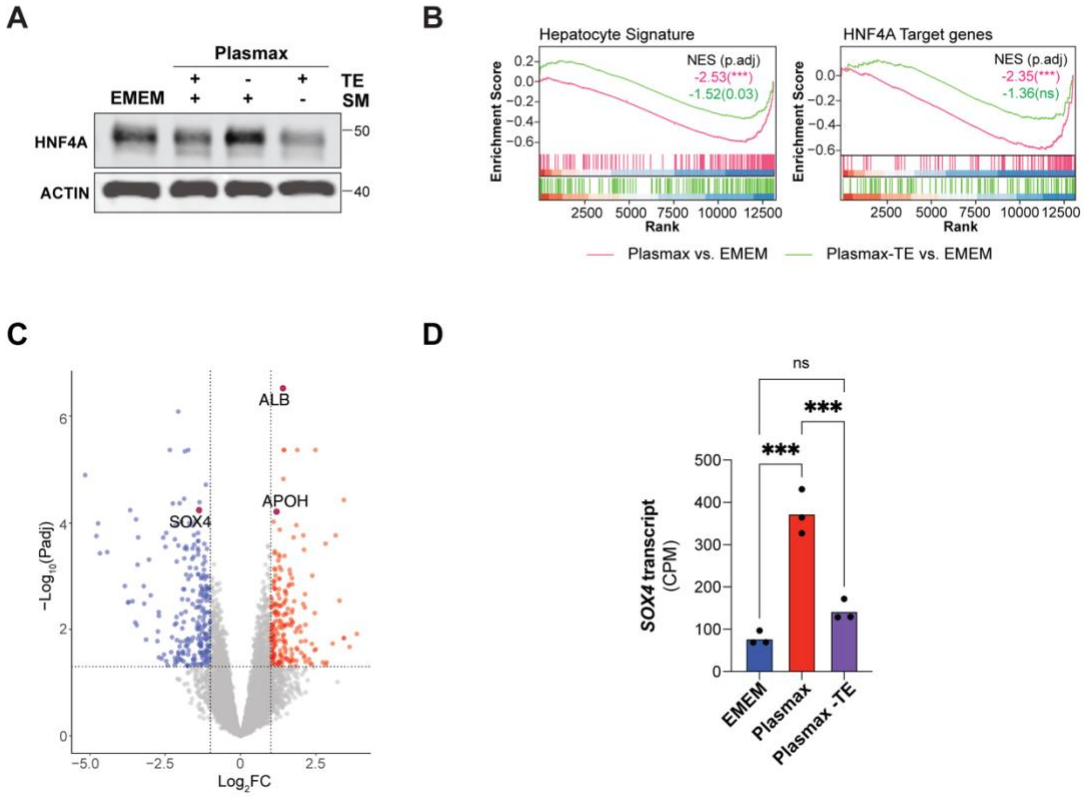

Figure 2. Trace element availability regulates hepatocyte differentiation
(A) Representative immunoblot analysis of HepG2 cells cultured in EMEM, Plasmax, Plasmax devoid of trace elements (TE) or Plasmax devoid of supplemental metabolites (SM). (B) GSEA plots derived from RNA-Seq analysis comparing HepG2 cells cultured in Plasmax with HepG2 cells cultured in EMEM or comparing HepG2 cells cultured in Plasmax-TE with HepG2 cells cultured in EMEM demonstrating signatures associated with hepatocyte cell state and function. (C) Volcano plot of DEGs identified from RNA-Seq analysis comparing HepG2 cells cultured in Plasmax-TE with HepG2 cells cultured in Plasmax, n=3. Hepatocyte differentiation markers are highlighted in maroon. Significantly upregulated genes are highlighted in red. Significantly downregulated genes are highlighted in blue. (D) *SOX4* transcript expression in counts per million (CPM) based on RNA-Seq analysis of HepG2 cells cultured in EMEM, Plasmax, or Plasmax-TE, n=3. For all experiments, ***P <0.001, ns = not significant.

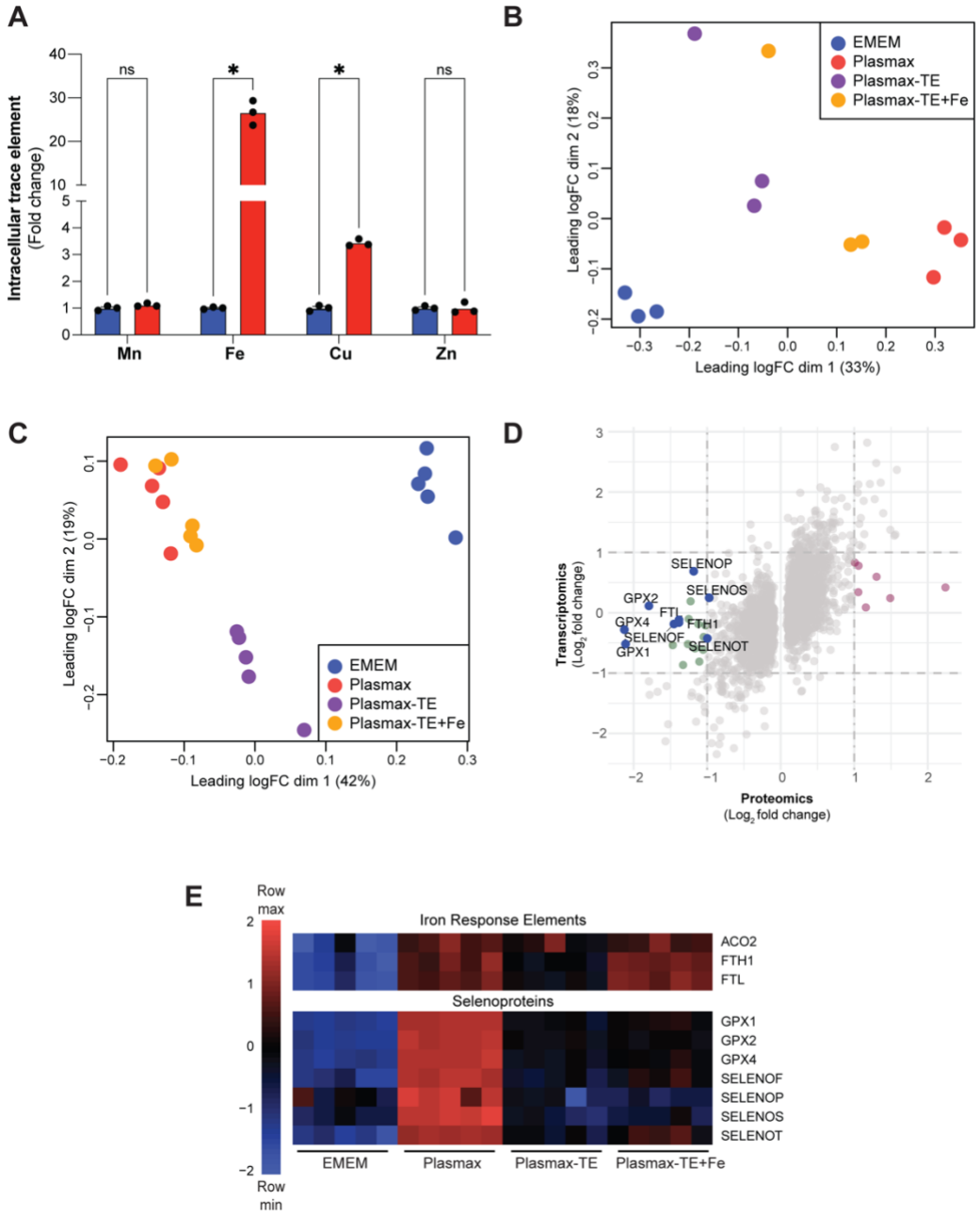

Figure 3. Multi-omics analysis reveals a relationship between trace element availability and metalloprotein expression

(A) Relative intracellular abundance of trace elements in HepG2 cells cultured in EMEM (blue) or Plasmax (red) n=3. (B) MDS plot of RNA-Seq data from HepG2 cells cultured in EMEM, Plasmax, Plasmax-TE, or Plasmax-TE supplemented with iron salts (0.12 μM ferric nitrate and 1.04 μM ferric sulfate; Plasmax-TE+Fe), n=3. (C) MDS plot of proteomic data from HepG2 cells cultured in EMEM, Plasmax, Plasmax-TE, or Plasmax-TE+Fe, n=5. (D) Correlation between proteomic and transcriptomic data from HepG2 cells cultured in Plasmax-TE with HepG2 cells cultured in Plasmax. Significantly differentially downregulated proteins whose transcripts were not significantly altered are highlighted in green. Significantly differentially upregulated proteins whose transcripts were not significantly altered are highlighted in magenta. Metalloproteins are highlighted in blue. (E) Heatmap of metalloprotein expression in HepG2 cells cultured in EMEM, Plasmax, Plasmax-TE or Plasmax-TE+Fe as determined by proteomic analysis, n=5. For all experiments, *P <0.05 , ns = not significant.

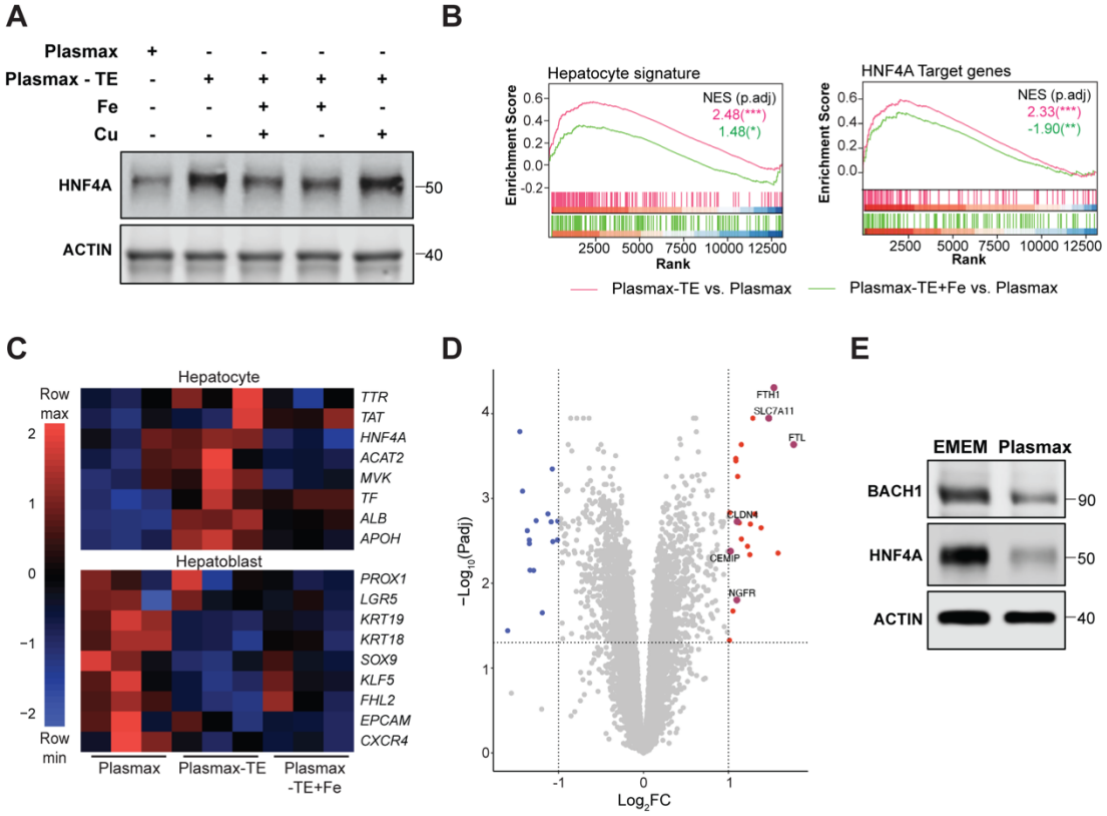

Figure 4. Iron availability contributes to the regulation of hepatocyte cell fate
(A) Representative immunoblot analysis of HepG2 cells cultured in Plasmax, Plasmax-TE, Plasmax-TE+Fe, Plasmax-TE supplemented with copper salts (0.005 μM cupric sulfate), or Plasmax-TE supplemented with iron and copper salts (0.12 μM ferric nitrate, 1.04 μM ferric sulfate, 0.005 μM cupric sulfate). (B) GSEA plots derived from RNA-Seq analysis comparing HepG2 cells cultured in Plasmax-TE with HepG2 cells cultured in Plasmax and comparing HepG2 cells cultured in Plasmax-TE+Fe with HepG2 cells cultured in Plasmax demonstrating signatures associated with hepatocyte cell state and function. (C) Heatmap of hepatocyte and hepatoblast gene expression in Plasmax, Plasmax-TE or Plasmax-TE+Fe as determined by RNA-Seq analysis, n=3. (D) Volcano plot of differentially expressed proteins identified from proteomic analysis comparing HepG2 cells cultured in Plasmax-TE+Fe with HepG2 cells cultured in Plasmax-TE, n=5. BACH1 targets are highlighted in maroon. Significantly upregulated proteins are highlighted in red. Significantly downregulated proteins are highlighted in blue. (E) Representative immunoblot analysis of HepG2 cells cultured in EMEM or Plasmax.

394 **References**
395

396 Addess KJ, Basilion JP, Klausner RD, Rouault TA & Pardi A (1997) Structure and dynamics
397 of the iron responsive element RNA: implications for binding of the RNA by iron
398 regulatory binding proteins. *J Mol Biol* 274: 72–83

399 Aden DP, Fogel A, Plotkin S, Damjanov I & Knowles BB (1979) Controlled synthesis of
400 HBsAg in a differentiated human liver carcinoma-derived cell line. *Nature* 282: 615–
401 616

402 Afgan E, Baker D, van den Beek M, Blankenberg D, Bouvier D, Čech M, Chilton J, Clements
403 D, Coraor N, Eberhard C, *et al* (2016) The Galaxy platform for accessible,
404 reproducible and collaborative biomedical analyses: 2016 update. *Nucleic Acids Res*
405 44: W3–W10

406 Ajioka RS, Phillips JD & Kushner JP (2006) Biosynthesis of heme in mammals. *Biochim*
407 *Biophys Acta* 1763: 723–736

408 Apiz Saab JJ, Dzierozynski LN, Jonker PB, AminiTabrizi R, Shah H, Menjivar RE, Scott AJ,
409 Nwosu ZC, Zhu Z, Chen RN, *et al* (2023) Pancreatic tumors exhibit myeloid-driven
410 amino acid stress and upregulate arginine biosynthesis. *Elife* 12

411 Arzumanian VA, Kiseleva OI & Poverennaya EV (2021) The curious case of the HepG2 cell
412 line: 40 years of expertise. *Int J Mol Sci* 22: 13135

413 Aziz N & Munro HN (1987) Iron regulates ferritin mRNA translation through a segment of its
414 5' untranslated region. *Proc Natl Acad Sci U S A* 84: 8478–8482

415 Boon R, Kumar M, Tricot T, Elia I, Ordovas L, Jacobs F, One J, De Smedt J, Eelen G, Bird
416 M, *et al* (12/2020) Amino acid levels determine metabolism and CYP450 function of
417 hepatocytes and hepatoma cell lines. *Nat Commun* 11: 1393

418 Cantor JR, Abu-Remaileh M, Kanarek N, Freinkman E, Gao X, Louissaint A Jr, Lewis CA &
419 Sabatini DM (2017) Physiologic medium rewires cellular metabolism and reveals uric
420 acid as an endogenous inhibitor of UMP synthase. *Cell* 169: 258-272.e17

421 Chambers I, Frampton J, Goldfarb P, Affara N, McBain W & Harrison PR (1986) The
422 structure of the mouse glutathione peroxidase gene: the selenocysteine in the active
423 site is encoded by the "termination" codon, TGA. *EMBO J* 5: 1221–1227

424 Charafe-Jauffret E, Ginestier C, Monville F, Finetti P, Adélaïde J, Cervera N, Fekairi S, Xerri
425 L, Jacquemier J, Birnbaum D, *et al* (2006) Gene expression profiling of breast cell
426 lines identifies potential new basal markers. *Oncogene* 25: 2273–2284

427 Chen L, Zhang C, Xue R, Liu M, Bai J, Bao J, Wang Y, Jiang N, Li Z, Wang W, *et al* (2024)
428 Deep whole-genome analysis of 494 hepatocellular carcinomas. *Nature* 627: 586–
429 593

430 Chen Y, Guo X, Zeng Y, Mo X, Hong S, He H, Li J, Fatima S & Liu Q (2023) Oxidative stress
431 induces mitochondrial iron overload and ferroptotic cell death. *Sci Rep* 13: 15515

432 Copeland PR (2003) Regulation of gene expression by stop codon recoding: selenocysteine.
433 *Gene* 312: 17–25

434 Davidson SM, Papagiannakopoulos T, Olenchock BA, Heyman JE, Keibler MA, Luengo A,
435 Bauer MR, Jha AK, O'Brien JP, Pierce KA, *et al* (2016) Environment impacts the
436 metabolic dependencies of Ras-driven non-small cell lung cancer. *Cell Metab* 23:
437 517–528

438 Demichev V, Messner CB, Vernardis SI, Lilley KS & Ralser M (2020) DIA-NN: neural
439 networks and interference correction enable deep proteome coverage in high
440 throughput. *Nat Methods* 17: 41–44

441 Dulbecco R & Freeman G (1959) Plaque production by the polyoma virus. *Virology* 8: 396–
442 397

443 Eagle H (1959) Amino acid metabolism in mammalian cell cultures. *Science* 130: 432–437

444 Flickinger KM, Wilson KM, Rossiter NJ, Hunger AL, Vishwasrao PV, Lee TD, Mellado Fritz
445 CA, Richards RM, Hall MD & Cantor JR (2024) Conditional lethality profiling reveals
446 anticancer mechanisms of action and drug-nutrient interactions. *Sci Adv* 10:
447 eadq3591

448 Gordillo M, Evans T & Gouon-Evans V (2015) Orchestrating liver development.
449 *Development* 142: 2094–2108

450 Gray NK & Hentze MW (1994) Iron regulatory protein prevents binding of the 43S translation
451 pre-initiation complex to ferritin and eALAS mRNAs. *EMBO J* 13: 3882–3891

452 Hentze MW, Caughman SW, Rouault TA, Barriocanal JG, Dancis A, Harford JB & Klausner
453 RD (1987) Identification of the iron-responsive element for the translational regulation
454 of human ferritin mRNA. *Science* 238: 1570–1573

455 Jiang X, Liu K, Jiang H, Yin H, Wang E-D, Cheng H, Yuan F, Xiao F, Wang F, Lu W, *et al*
456 (2023) SLC7A14 imports GABA to lysosomes and impairs hepatic insulin sensitivity
457 via inhibiting mTORC2. *Cell Rep* 42: 111984

458 Kao Y-R, Chen J, Kumari R, Ng A, Zintiridou A, Tatiparthy M, Ma Y, Aivalioti MM, Moulik D,
459 Sundaravel S, *et al* (2024) An iron rheostat controls hematopoietic stem cell fate. *Cell*
460 *Stem Cell* 31: 378-397.e12

461 Katsuda T, Sussman JH, Ito K, Katznelson A, Yuan S, Takenaka N, Li J, Merrell AJ, Cure H,
462 Li Q, *et al* (2024) Cellular reprogramming in vivo initiated by SOX4 pioneer factor
463 activity. *Nat Commun* 15: 1761

464 Kaur S, Kidambi S, Ortega-Ribera M, Thuy LTT, Nieto N, Cogger VC, Xie W-F, Tacke F &
465 Gracia-Sancho J (2023) In vitro models for the study of liver biology and diseases:
466 Advances and limitations. *Cell Mol Gastroenterol Hepatol* 15: 559–571

467 Kitamuro T, Takahashi K, Ogawa K, Udono-Fujimori R, Takeda K, Furuyama K, Nakayama
468 M, Sun J, Fujita H, Hida W, *et al* (2003) Bach1 functions as a hypoxia-inducible
469 repressor for the heme oxygenase-1 gene in human cells. *J Biol Chem* 278: 9125–
470 9133

471 Kolde R (2012) Pheatmap: pretty heatmaps. *R package version*

472 Kryukov GV, Castellano S, Novoselov SV, Lobanov AV, Zehtab O, Guigó R & Gladyshev VN
473 (2003) Characterization of mammalian selenoproteomes. *Science* 300: 1439–1443

474 Law CW, Chen Y, Shi W & Smyth GK (2014) voom: Precision weights unlock linear model
475 analysis tools for RNA-seq read counts. *Genome Biol* 15: R29

476 Lignitto L, LeBoeuf SE, Homer H, Jiang S, Askenazi M, Karakousi TR, Pass HI, Bhutkar AJ,
477 Tsirigos A, Ueberheide B, *et al* (2019) Nrf2 Activation Promotes Lung Cancer
478 Metastasis by Inhibiting the Degradation of Bach1. *Cell* 178: 316-329.e18

479 Lin C-Y, Chang T-W, Hsieh W-H, Hung M-C, Lin I-H, Lai S-C & Tzeng Y-J (2016)
480 Simultaneous induction of apoptosis and necroptosis by Tanshinone IIA in human
481 hepatocellular carcinoma HepG2 cells. *Cell Death Discov* 2: 16065

482 Liu F, Tian T, Zhang Z, Xie S, Yang J, Zhu L, Wang W, Shi C, Sang L, Guo K, *et al* (2022)
483 Long non-coding RNA SNHG6 couples cholesterol sensing with mTORC1 activation
484 in hepatocellular carcinoma. *Nat Metab* 4: 1022–1040

485 Liu Z, Xu Y, Zhang W, Gao X, Luo G, Song H, Liu J & Wang H (2021) Identification of targets
486 of JS-K against HBV-positive human hepatocellular carcinoma HepG2.2.15 cells with
487 iTRAQ proteomics. *Sci Rep* 11: 10381

488 López-Terrada D, Cheung SW, Finegold MJ & Knowles BB (2009) Hep G2 is a
489 hepatoblastoma-derived cell line. *Hum Pathol* 40: 1512–1515

490 Muir A, Danai LV, Gui DY, Waingarten CY, Lewis CA & Vander Heiden MG (2017)
491 Environmental cystine drives glutamine anaplerosis and sensitizes cancer cells to
492 glutaminase inhibition. *Elife* 6: e27713

493 Müller S, Sindikubwabo F, Cañeque T, Lafon A, Versini A, Lombard B, Loew D, Wu T-D,
494 Ginestier C, Charafe-Jauffret E, *et al* (2020) CD44 regulates epigenetic plasticity by
495 mediating iron endocytosis. *Nat Chem* 12: 929–938

496 Neve RM, Chin K, Fridlyand J, Yeh J, Baehner FL, Fevr T, Clark L, Bayani N, Coppe J-P,
497 Tong F, *et al* (2006) A collection of breast cancer cell lines for the study of functionally
498 distinct cancer subtypes. *Cancer Cell* 10: 515–527

499 Ogawa K, Sun J, Taketani S, Nakajima O, Nishitani C, Sassa S, Hayashi N, Yamamoto M,
500 Shibahara S, Fujita H, *et al* (2001) Heme mediates derepression of Maf recognition
501 element through direct binding to transcription repressor Bach1. *EMBO J* 20: 2835–
502 2843

503 Ong AJS, Bladen CE, Tigani TA, Karamalakis AP, Evason KJ, Brown KK & Cox AG (2023)
504 The KEAP1-NRF2 pathway regulates TFEB/TFE3-dependent lysosomal biogenesis.
505 *Proc Natl Acad Sci U S A* 120: e2217425120

506 Oyake T, Itoh K, Motohashi H, Hayashi N, Hoshino H, Nishizawa M, Yamamoto M & Igarashi
507 K (1996) Bach proteins belong to a novel family of BTB-basic leucine zipper
508 transcription factors that interact with MafK and regulate transcription through the NF-
509 E2 site. *Mol Cell Biol* 16: 6083–6095

510 Park S, Park J-H, Jung H-J, Jang J-H, Ahn S, Kim Y, Suh P-G, Chae S, Yoon JH, Ryu SH, *et*
511 *al* (2018) A secretome profile indicative of oleate-induced proliferation of HepG2
512 hepatocellular carcinoma cells. *Exp Mol Med* 50: 1–14

513 Parviz F, Matullo C, Garrison WD, Savatski L, Adamson JW, Ning G, Kaestner KH, Rossi
514 JM, Zaret KS & Duncan SA (2003) Hepatocyte nuclear factor 4alpha controls the

515 development of a hepatic epithelium and liver morphogenesis. *Nat Genet* 34: 292–
516 296

517 Pyun J, McInnes LE, Donnelly PS, Mawal C, Bush AI, Short JL & Nicolazzo JA (2022)
518 Copper bis(thiosemicarbazone) complexes modulate P-glycoprotein expression and
519 function in human brain microvascular endothelial cells. *J Neurochem* 162: 226–244

520 Rao X, Huang X, Zhou Z & Lin X (2013) An improvement of the 2ˆ(-delta delta CT) method
521 for quantitative real-time polymerase chain reaction data analysis. *Biostat Bioinform*
522 *Biomath* 3: 71–85

523 Rawat V, DeLear P, Prashanth P, Ozgurses ME, Tebeje A, Burns PA, Conger KO, Solís C,
524 Hasnain Y, Novikova A, *et al* (2024) Drug screening in human physiologic medium
525 identifies uric acid as an inhibitor of rigosertib efficacy. *JCI Insight* 9

526 Sanghvi VR, Leibold J, Mina M, Mohan P, Berishaj M, Li Z, Miele MM, Lailler N, Zhao C, de
527 Stanchina E, *et al* (2019) The Oncogenic Action of NRF2 Depends on De-glycation
528 by Fructosamine-3-Kinase. *Cell* 178: 807-819.e21

529 Sekiya S & Suzuki A (2011) Direct conversion of mouse fibroblasts to hepatocyte-like cells
530 by defined factors. *Nature* 475: 390–393

531 Senkowski W, Gall-Mas L, Falco MM, Li Y, Lavikka K, Kriegbaum MC, Oikkonen J, Bulanova
532 D, Pietras EJ, Voßgröne K, *et al* (2023) A platform for efficient establishment and
533 drug-response profiling of high-grade serous ovarian cancer organoids. *Dev Cell* 58:
534 1106-1121.e7

535 Shen M, Goforth JB & Eisenstein RS (2023) Iron-dependent post transcriptional control of
536 mitochondrial aconitase expression. *Metallomics* 15

537 Smyth GK (2005) limma: Linear Models for Microarray Data. In *Bioinformatics and*
538 *Computational Biology Solutions Using R and Bioconductor* pp 397–420. New York:
539 Springer-Verlag

540 Sun J, Hoshino H, Takaku K, Nakajima O, Muto A, Suzuki H, Tashiro S, Takahashi S,
541 Shibahara S, Alam J, *et al* (2002) Hemoprotein Bach1 regulates enhancer availability
542 of heme oxygenase-1 gene. *EMBO J* 21: 5216–5224

543 Tardito S, Oudin A, Ahmed SU, Fack F, Keunen O, Zheng L, Miletic H, Sakariassen PØ,
544 Weinstock A, Wagner A, *et al* (2015) Glutamine synthetase activity fuels nucleotide
545 biosynthesis and supports growth of glutamine-restricted glioblastoma. *Nat Cell Biol*
546 17: 1556–1568

547 Vande Voorde J, Ackermann T, Pfetzer N, Sumpton D, Mackay G, Kalna G, Nixon C, Blyth K,
548 Gottlieb E & Tardito S (2019) Improving the metabolic fidelity of cancer models with a
549 physiological cell culture medium. *Sci Adv* 5: eaau7314

550 Wei X, Guo J, Li Q, Jia Q, Jing Q, Li Y, Zhou B, Chen J, Gao S, Zhang X, *et al* (2019) Bach1
551 regulates self-renewal and impedes mesendodermal differentiation of human
552 embryonic stem cells. *Sci Adv* 5: eaau7887

553 Wickham H (2016) ggplot2: Elegant Graphics for Data Analysis Cham: Springer International
554 Publishing

555 Wiel C, Le Gal K, Ibrahim MX, Jahangir CA, Kashif M, Yao H, Ziegler DV, Xu X, Ghosh T,
556 Mondal T, *et al* (2019) BACH1 Stabilization by Antioxidants Stimulates Lung Cancer
557 Metastasis. *Cell* 178: 330-345.e22

558 Yang S, Ooka M, Margolis RJ & Xia M (2023) Liver three-dimensional cellular models for
559 high-throughput chemical testing. *Cell Rep Methods* 3: 100432

560 Yu G, Wang L-G, Han Y & He Q-Y (2012) clusterProfiler: an R package for comparing
561 biological themes among gene clusters. *OMICS* 16: 284–287

562 Zhang Z-L, Liu G-C, Peng L, Zhang C, Jia Y-M, Yang W-H & Mao L (2018) Effect of PAK1
563 gene silencing on proliferation and apoptosis in hepatocellular carcinoma cell lines
564 MHCC97-H and HepG2 and cells in xenograft tumor. *Gene Ther* 25: 284–296

565 Zhuang X, Wang Q, Joost S, Ferrena A, Humphreys DT, Li Z, Blum M, Krause K, Ding S,
566 Landais Y, *et al* (2025) Ageing limits stemness and tumorigenesis by reprogramming
567 iron homeostasis. *Nature* 637: 184–194

568 Zinoni F, Birkmann A, Stadtman TC & Böck A (1986) Nucleotide sequence and expression of
569 the selenocysteine-containing polypeptide of formate dehydrogenase (formate-
570 hydrogen-lyase-linked) from Escherichia coli. *Proc Natl Acad Sci U S A* 83: 4650–
571 4654